THE IMPACT OF HIP PROCESS AND HEAT TREATMENT ON THE MECHANICAL BEHAVIOUR OF AN Al–Si–Mg ALLOY COMPONENT

Toni Bogdanoff [iD], Ehsan Ghassemali, Anders E. W. Jarfors and Salem Seifeddine
Department of Materials and Manufacturing, Jönköping University, Box 1026, 55111 Jönköping, Sweden

Abstract

This study investigates the effect of hot isostatic pressing (HIPping) on the static and fatigue properties of sand-casting A356 aluminium alloys. HIPping is a method to improve the fatigue properties in aluminium cast material by reducing or eliminating the inner porosities. Investigation of the complex interaction between the microstructural features on mechanical properties before and after the HIPping process was examined using computed tomography and scanning electron microscopy (SEM). Castings generally contain pores and defects that have a detrimental impact on the fatigue properties. The HIPping process closes the porosities in all investigated samples with an increase in density. Without significant defects, the mechanical performance improved in the finer microstructure. However, a considerable variation in the results was found between the different conditions, whereas the coarser microstructure with larger porosities before HIPping showed remarkably reduced results. The high-cycle fatigue-tested samples showed reduced fatigue propagation zone in the coarser microstructure. Moreover, large cleavage areas containing bifilms in the fracture surfaces indicate that the healing process of porosities is inefficient. These porosities are closed but not healed, resulting in a detrimental effect on the static and dynamic properties.

Keywords: *hot isostatic pressing (HIP), heat treatment, castings, fatigue properties, Al–Si alloys*

Introduction

The strive for lightweight in the automotive sector has increased over the last decade because of the demand for reducing gas emissions and fuel consumption. Moreover, electric vehicles require more optimised mechanical performance with weight reduction in complex components since they affect the driving distance. Hypoeutectic aluminium–silicon (Al–Si) cast alloys are attractive in terms of lightweight, excellent castability, and high strength-to-weight ratio. These alloys could be valid candidates for components exposed to cyclic loading in the automotive industry. Unfortunately, the porosity and defects from the casting process have a detrimental effect on the mechanical properties.[1,2] Components in critical applications require improved mechanical properties, which can be achieved either with pre-solidification treatments, such as grain refinement and eutectic modification,[3–5] or post-solidification treatments, like heat treatment[6] and hot isostatic pressing (HIPping).[7,8]

In cast Al-Si alloys, one issue could be porosity, which is one of the main initiation sites for fatigue cracks. Moreover, oxides and surface roughness are also critical factors for fatigue properties. Depending on the casting method, the component could contain different amounts and porosity sizes, affecting the mechanical properties. Even a small amount of porosity has significantly affected the fatigue properties in Al-Si alloys.[9] Research has shown that the presence of bifilms is responsible for the development of pores in aluminium castings. The process leading to pore formation involves bifilms being captured in the casting and later expanding under the influence of negative pressures generated during solidification and/or the infiltration of hydrogen into the bifilms.[10–12] HIPping is a method to reduce the internal porosity within a component, which

improves the mechanical properties and, most of all, the fatigue strength. Moreover, the HIPping process has a negligible effect on microstructural features like grain size and secondary dendrite arm spacing (SDAS).[13,14] The process involves heating the castings to 60–90 % of the absolute solidus temperature and applying an isostatic gas pressure.[15] Exceeding the temperature during HIPping can result in detrimental effects such as incipient melting or coarsening.[16] Several researchers have shown that the HIPping process in aluminium castings successfully densified the parts by eliminating the porosity with improved mechanical properties.[16–18] However, Zhou et al.[19] showed that the initial contents of shrinkage porosity in magnesium alloys are the determining factor for the effectiveness of the HIPping process. The silicon (Si) particle morphology and size affect the mechanical properties, both static and dynamic. These Si particles are influenced by the HIPping and heat treatment process, which coarsen and spheroidize the particles.[13] Moreover, before high-temperature treatment, the size of the Si particles affects the heat treatment process time. Usually, fine fibrous Si particles are preferable since they reduce the heat treatment time.[20]

The work presented herein investigated the effect of HIPping combined with heat treatment on the static mechanical properties and cyclic behaviour of Al–7Si–Mg alloys. Computed tomography (CT) scanning and density measurement of the different thicknesses in as-cast, HIPed, and heat-treated conditions aims to identify the effect of HIPping on mechanical properties. In situ cyclic testing using a scanning electron microscope (SEM) highlights the interaction between crack development and microstructural features. The size of porosities before the HIPping significantly affects the crack propagation, a parameter to consider. This understanding of the effect of the HIPping process will provide knowledge to increase the usage of Al-Si components in structural applications.

Experimental Procedure

A commercial EN AB 42000 alloy (A356) was melted in an electric melting furnace in a sand-casting foundry. After melting, grain refiner (NUCLEANT 1582) and Si modifier (SIMODAL 1576) were added using an automated melt treatment station (FOSECO MTS 1500) following the standard practice in the melting operation at the foundry. Table 1 reports the chemical composition evaluated with a Spectromaxx CCD LMXM3 optical emission spectrometer (OES).
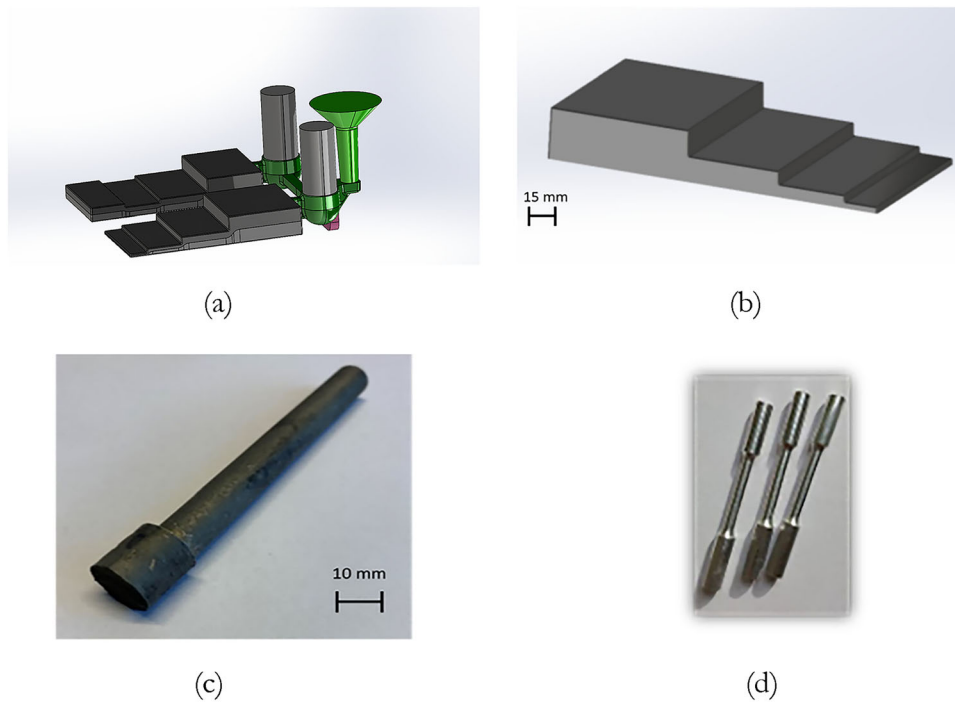
The components studied are stair castings with different thicknesses, as shown in Figure 1a, produced by uncoated sand mould casting using ALPHASET RESIN TPA75. The circles in Figure 1b highlight the location of the extracted samples.

Samples from the thicknesses 16 and 32 mm were machined to a diameter of 12 mm and length of 100 mm (see Figure 1c) exposed to HIPping at 540 °C for 2 hours with a pressure of 75 MPa. Solution heat treatment was performed at 540 °C for 10 hours, followed by quench in the water at 50 °C. After 36 hours of natural ageing, artificial ageing followed at 170 °C for 12 hours. The parameters for the artificial ageing time were performed with Brinell hardness testing. CT scanning was conducted in the as-cast condition, after HIPping, and after the solution heat treatment. The detection limit of the CT scanning is 0.25 mm in diameter.

The microstructure was studied using an optical microscope (Olympus GX71) and a scanning electron microscope (Tescan Lyra 4). The SDAS was measured at ten locations at each thickness. The grain size was measured by the intercept method according to ASTM E112-96. The fractographic examination of the post-mortem specimens was performed by using the scanning electron microscope with energy-dispersive X-ray spectroscopy (EDS–Octane Pro, Edax).

The density was measured on 20 samples in each condition and calculated using the Archimedes principle.

Tensile and fatigue specimens were machined from the heat-treated material into cylindrical test specimens with a gauge length of 36 mm and a diameter of 6 mm see Figure 1d. Tensile testing was carried out at room temperature, following the ASTM E8 standard, with a constant crosshead speed of 0.5 mm/min. A minimum of four samples for each condition was tested with a clip-on extensometer to measure the strain. Miniature compact-tension (MCT) samples were cut by an electron discharge machining method with a 0.25-mm wire. The dimensions of the MCT sample, as shown in Figure 2a, were designed starting from the ASTM E647-00 Standard guidelines. In situ cyclic tests were performed on the Kammrath and Weiss stage, see Figure 2b inside the TESCAN Lyra3 SEM at room temperature. Before cyclic loading, monotonic tension loading up to failure showed that the critical stress intensity factor Kc. The selected ΔK with a constant load ratio (R) of 0.2 was used, with the loading speed of 8 μm/s ($\sim$ 0.1 Hz). The field-of-view (FOV) size was 300 μm $\times$ 300 μm, and it comprehended the notch tip to investigate the crack development.

Table 1. Chemical Composition (wt.%) of the Investigated Alloy

Alloy	Si	Mg	Cu	Fe	Ti	Na	Al
42100	7.4	0.36	0.01	0.11	0.13	0.013	Balance

Figure 1. *(a) Stair casting; (b) location of the extracted samples; (c) extracted sample for HIPping, heat treatment and CT scanning; (d) samples for static and dynamic testing.*
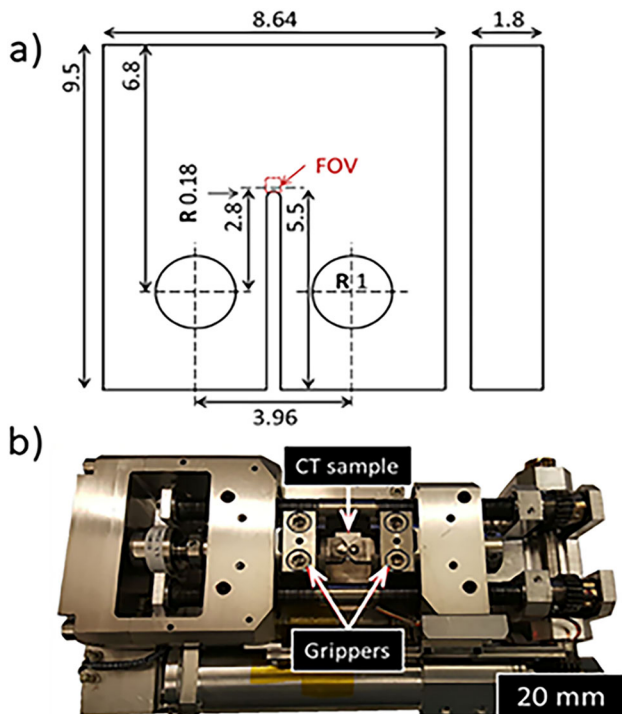
Figure 2. *(a) Dimensions of the MCT sample in mm; (b) miniature stage for in situ cyclic tests.*

Fatigue testing was carried out using the staircase method according to ISO 12107. The maximum number of cycles was set to $2*10^6$ at a frequency of 50 Hz. The fatigue tests were conducted at room temperature on the combined HIPed and heat-treated material.

Results and Discussion

Microstructure

Figure 3 illustrates the microstructures of the staircase casting Al–7Si–0.3Mg alloy in the as-cast condition. The secondary dendrite arm spacing (SDAS) for the investigated stair thicknesses 16 mm and 32 mm is 58 ± 6 μm and 81 ± 7 μm. At the same time, the grain size was measured to 261 μm for the 16 mm and 416 μm for the 32 mm thickness. The coarser microstructure shows a more inhomogeneous modification level because of the slow cooling rate highlighted in Figure 3b. Moreover, a significant difference in porosity size between the two conditions is visible in the micrographs in Figure 3, confirmed by the density measurements in Table 2 with lower density in the coarser microstructure. Observation shows both gas and shrinkage porosities in the different microstructures, these defects are related to mould filling, where entrapped air is captured in the molten metal, forming gas porosities and feeding-related shrinkage porosities.

Natural ageing of 36 hours after the solution treatment was selected, which is beneficial for Al–Si–Mg alloys. It promotes a microstructure with a lower number density of coarser particles than the directly aged material.[21,22] The
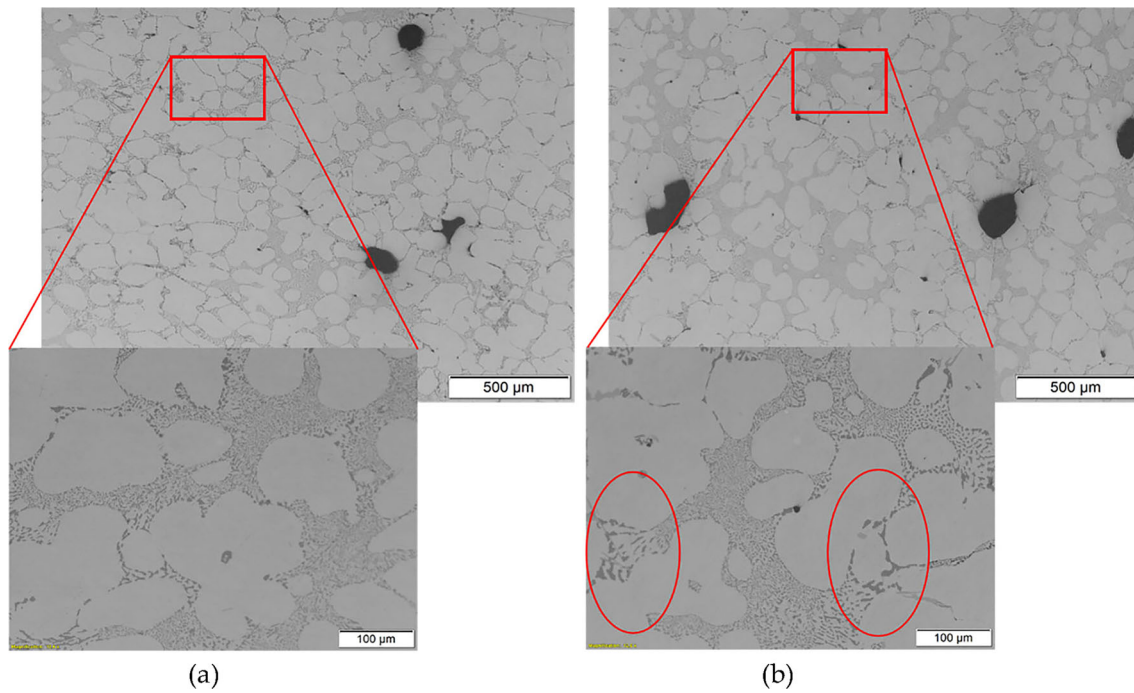
Figure 3. *Microstructures of the Al–7Si–Mg alloy, (a) as-cast condition 16 mm thickness, (b) as-cast condition 32 mm thickness.*

Table 2. *Average Values and Standard Deviations of Density and Area of Porosity from the CT Scanning*

	As-cast 16 mm	As-cast 32 mm	HIPed 16 mm	HIPed 32 mm	HIPed + T6 16 mm	HIPed + T6 32 mm
Density	2.655	2.650	2.671	2.67	2.67	2.67
CT scanning area porosity %	0.28	0.71	0.01	0.00	0.02	0.00

chosen artificial ageing time of 12 hours was selected from the hardness test of the material exposed for artificial ageing at 170 °C in the time interval from 0 h to 1000 h, as shown in Figure 4. These values are in the range of work done by Ceschini et al.[14] Artificial ageing was selected to reach the peak strength of the material.

The micrographs in Figure 5 show the HIPed and heat-treated material with spheroidized and coarsened Si particles as reported in the literature[20,23] and no observed porosities in the different conditions. Figure 5b shows the micrograph of the 32 mm heat-treated alloy that contains areas with coarser Si particles, although the Na additions were in the recommended range.[24–26] The slow cooling rate in the 32 mm thickness leads to such an inhomogeneous Si distribution because of back diffusion.[22]

The prepared samples were CT scanned in as-cast, after HIPping, and after heat treatment conditions, as shown in Figure 6. The amount of detected porosity in the as-cast condition of the 32 mm thickness shows significantly
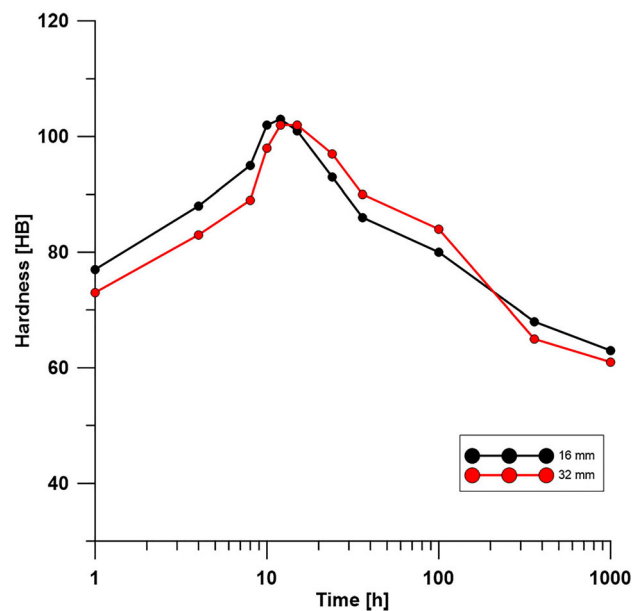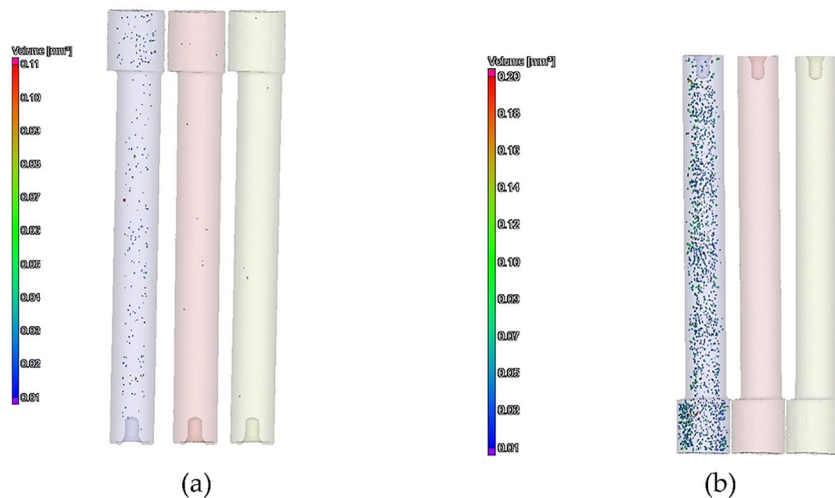

Figure 4. *The hardness response of the artificial ageing times on the staircase component at 170 °C*
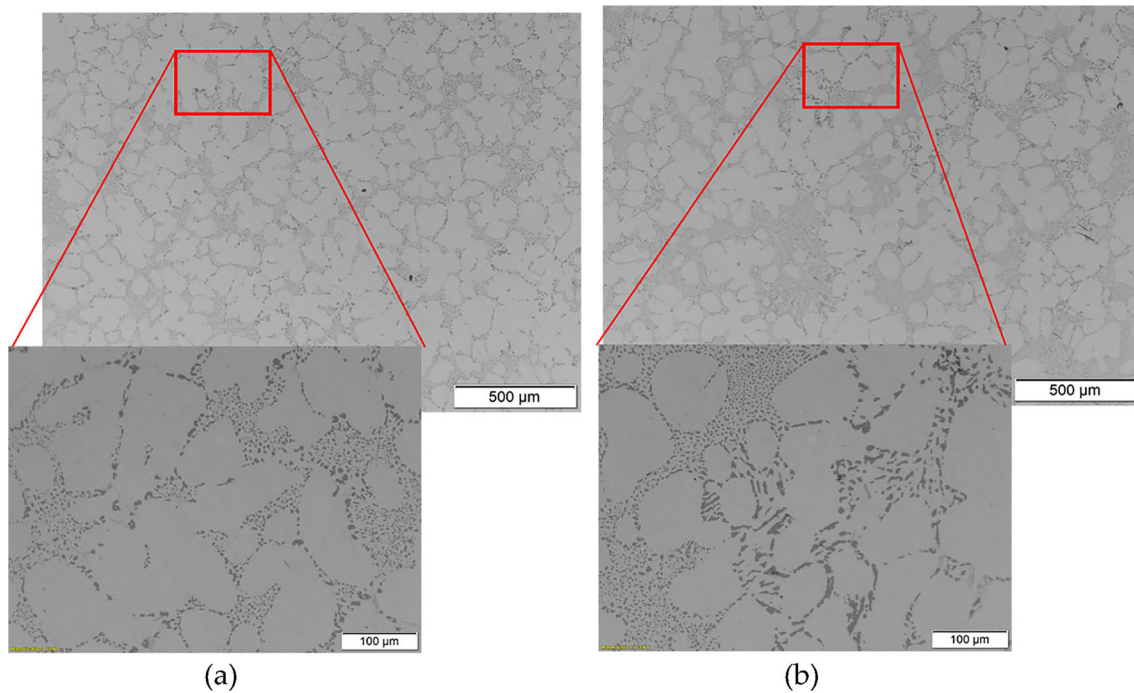
Figure 5. Microstructures of the Al–7Si–Mg alloy, (a) heat-treated condition 16 mm thickness, (b) heat-treated condition 32 mm thickness.


Figure 6. CT scanning of the material in as-cast (blue), HIPed (red), and heat-treated (green). (a) 16 mm, (b) 32 mm.

higher porosity content than the limit of detection (0.25 mm in diameter) compared to the 16 mm condition (Table 2), which correlates well with the observation in the micrographs Figure 3.

The HIPping process affects the material (red), as shown in Figure 6, and still detects porosity larger than 0.25 mm in diameter in the samples. However, the porosity area larger than 0.25 mm in diameter is nearly zero in all HIPed material. Furthermore, after the HIPping process, the specimens were exposed to the high solution treatment temperature, which showed no indication that the pores larger than 0.25 mm in diameter were opening up (green). These results agree with the density of the HIPed + heat-treated material. The micrographs after Hipping and heat treatment (Fig 5), CT scanning (Fig 6), and density results (Table 2) show that the porosities are closed by the HIPping process as reported in the literature.[8,27,28]
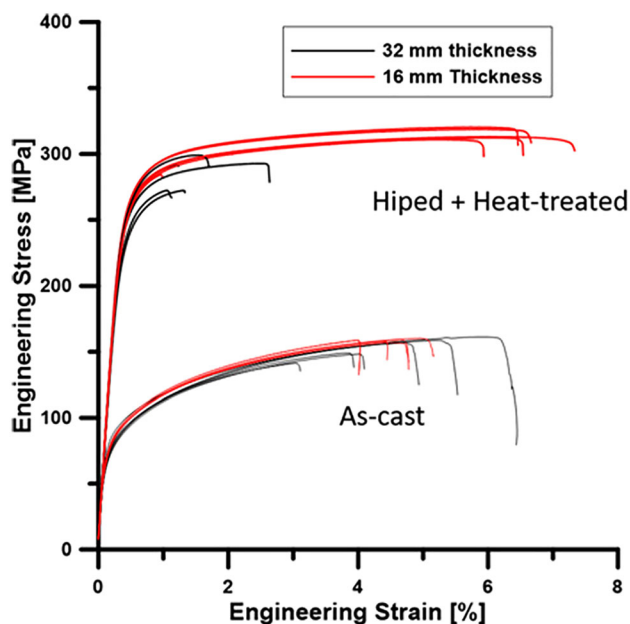
Figure 7. Tensile properties in the as-cast and HIPed + heat-treated samples.

Table 3. Average Values and Standard Deviations of Mechanical Properties in the as-cast and HIPed +heat-Treated Conditions

Alloy condition	As-cast		HIPed + heat-treated	
	16 mm	32 mm	16 mm	32 mm
Fatigue strength (MPa)			142 ± 3.5	127 ± 3.5
UTS (MPa)	159 ± 1.5	148 ± 6.5	315 ± 4	285 ± 11
YS (MPa)	91.2 ± 1.5	91.3 ± 5.7	271 ± 5	261 ± 10
Elongation (%)	4.6 ± 0.4	4.6 ± 1.1	5.9 ± 0.5	1.1 ± 0.5
Ratio			0.45	0.44

Mechanical Properties

The tensile testing results in the as-cast condition, as shown in Figure 7, indicate a minor difference in ultimate tensile strength (UTS) and yield strength (YS) between the two tested conditions. This minor difference in UTS could be related to the coarseness of the material with a difference in both SDAS and grain size showing a 7–10 % improvement with reduced SDAS and grain size.

However, a more extensive spread in the elongation to failure is detected in the coarser microstructure, even having samples showing the highest elongation to failure with up to 6 %. This variation could be related to the location of the defects within the samples. These results agree with Riestra et al.[3], which showed a similar improvement of elongation to failure with a modified and grain-refined coarser microstructure produced in Bridgman equipment. In this case, the larger dendrites are more prone to deform without affecting the surrounding particles. Results after HIPping and heat treatment show a remarkable difference between the investigated conditions. In contrast, the 16 mm specimen shows an improved elongation to failure from 4 to 6 % and more consistency within the analysed samples. A remarkable decrease in elongation is detected in the 32 mm samples from the as-cast condition 4.6 % ± 1.1 down to 1.1 % ± 0.5. These elongation differences to failure are related to increased strength in the α-Al matrix, more extensive intermetallic phases, and bifilms. Moreover, the reduction in elongation to failure in the 32 mm samples could be because of the double-oxide films that have more time to unfurl during solidification in the coarser microstructure, resulting in larger areas of oxide surfaces which are not bonding completely in the HIPping
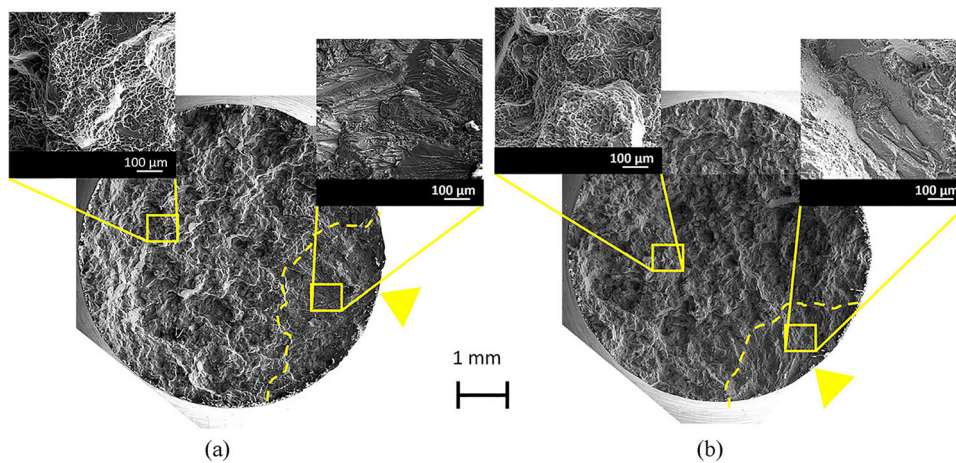
process. The HIPed and heat-treated conditions increase the YS almost three times and UTS up to twice from the as-cast conditions, see Table 3. This is due to precipitation hardening from the heat treatment process. Moreover, the standard deviation in the results is significantly more prominent in the coarser microstructure for both conditions.

The fatigue strength of the HIPed and heat-treated specimens followed the same trend as the UTS, with an 11 % higher for the 16 mm material. These results contradict the literature, stating that the fatigue life increases with SDAS larger than 60 μm in heat-treated conditions.[29] The ratio between fatigue strength and UTS is 0.44 and 0.45 on the different conditions, which agrees with the literature.[30]
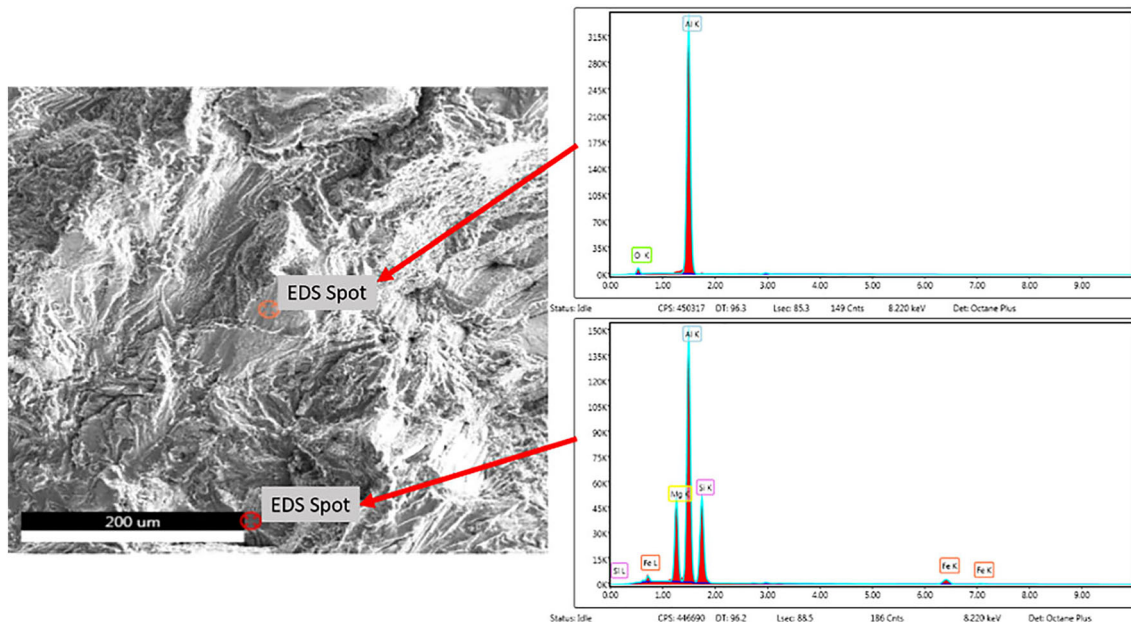
Fracture Surface Investigation

The fracture surfaces of the fatigue specimen in Figure 8 showed the initiation point (yellow arrow) with the following propagation zone and a final failure zone. All the fracture surfaces show that the cracks initiated at or near the specimen surface. The 16 mm sample, see Figure 8a, has a significantly larger propagation zone than the 32 mm, see Figure 8b. The 32 mm fracture surface has more brittle cleavage areas than the 16 mm samples in the propagation zone, and these cleavage areas are either Fe-phases or oxides measured with the EDS, as shown in Figure 9. The area of oxides results from closed porosities not healed in the HIPping process. The final failure zone shows a mixed ductile and brittle fracture surface mode.

The fracture profile of the specimen in the as-cast condition shows that the failure followed the eutectic regions and intermetallic phases in the 16 mm condition, see Figure 10a; in the 32 mm condition, see Figure 10b. Porosities

Figure 8. The fracture surface of the HIPed and heat-treated material. The yellow arrow shows the initiation sites. The dashed yellow lines indicate the end of the propagation zone. (a) 16 mm and (b) 32 mm.

**Figure 9.** The fracture surface of the 32 mm specimen with two EDS spot measurements.

from the casting are rarely observed below the fracture profile in the investigated samples in Figure 10.

The 16 mm specimens in the HIPed and heat-treated condition showed a similar fracture profile as the as-cast specimens, see Figure 11a. However, the fracture profile in the 32 mm specimen follows eutectic, intermetallics phases, and bifilms, see Figure 11b. Moreover, in the 32 mm condition, areas following other features produce cleavage regions in the propagation caused by larger intermetallics or bifilms, see Figure 11c. Bifilms are detected close to the fracture profile, see Figure 11d. These bifilms are from the molten metal before casting and are not cleaned throughout the degassing and fluxing and follow into the final component.

In situ Cyclic Testing

In situ cyclic testing belongs to the low-cycle fatigue regime, as the samples survived 340–1500 cycles. The fatigue crack initiation in hypoeutectic Al-Si casting alloys usually results from defects at the surface and subsurface levels. However, with limited defects, crack initiation nucleates generally from surface roughness, discontinuities such as slip bands, or particle debonding/breakage. In the 16 mm samples, after the preload in Figure 12a, no visible cracks are observed in the FOV. Figure 12b shows that after 600 cycles, an indication of the crack initiation from slip bands at the notch appears. At 740 cycles, crack propagation followed the eutectic regions and slip bands in the FOV, see Figure 12c. The propagation continues to
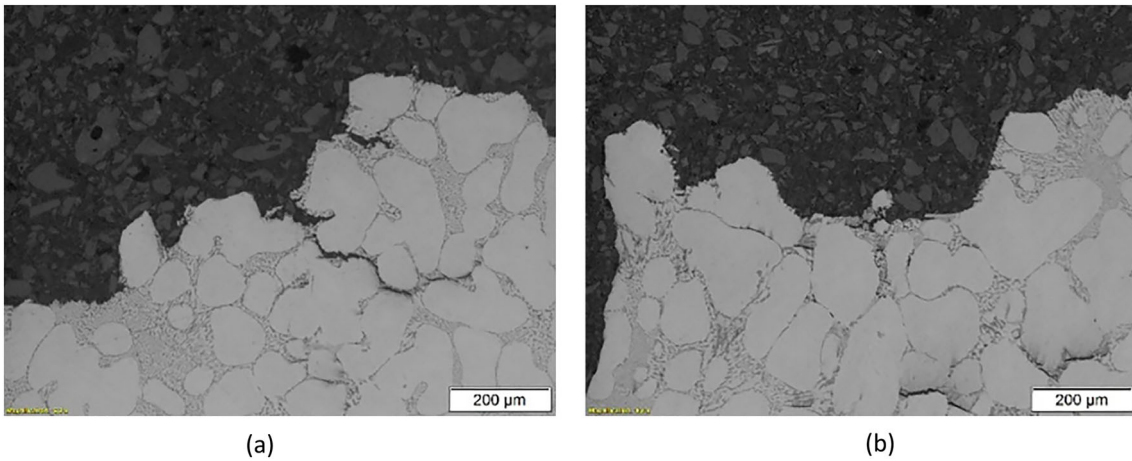
**Figure 10.** *Fracture profile of the investigated as-cast conditions, (a) 16 mm and (b) 32 mm.*
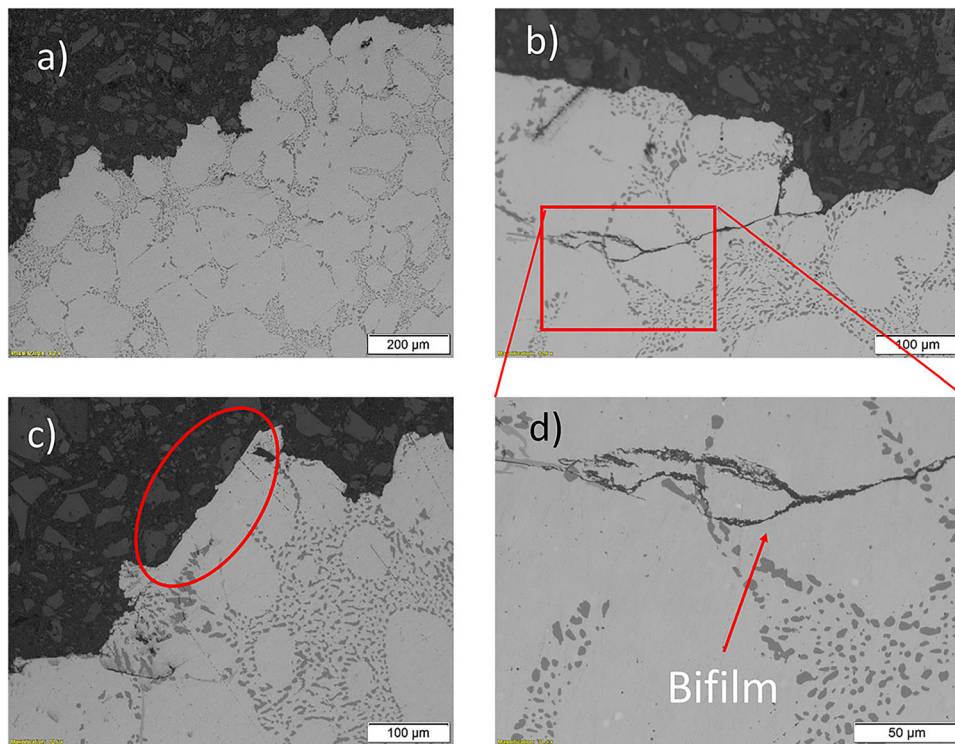
Figure 11. *Fracture profile of the heat-treated conditions, (a) 16 mm, (b) 32 mm containing bifilm, (c) 32 mm specimen highlighting cleavage, and (d) enlarged micrograph of (b).*

follow the eutectic regions until failure. No cracks were observed in the 32 mm specimens after 300 cycles in the FOV, see Figure 12d. However, a crack opens up in an area away from the notch, see Figure 12e. The orientation of the visible cracks is preferable in the perpendicular direction to the loading. This phenomenon has been observed in other literature, showing that bifilms open up and are responsible for nucleation of intermetallic phases.[31] Continuous cyclic loading increases the growth of the crack, and an increased amount of crack particles are detected in the FOV, see Figure 12f. However, the final failure is the large crack that opened up after 300 cycles away from the notch linked

with the rapid propagation path. This could explain the reduced propagation zone in the fracture surface in Figure 8b. The 32-mm specimen consists of regions, whereas the crack followed the eutectic and cleavage of intermetallics. Moreover, the significant difference in mechanical properties between the conditions indicates that the porosity difference before HIPping affects the propagation path. These defects not eliminated with the HIPping process were confirmed with the fracture profile, and fracture surface investigations are detrimental to the mechanical properties.
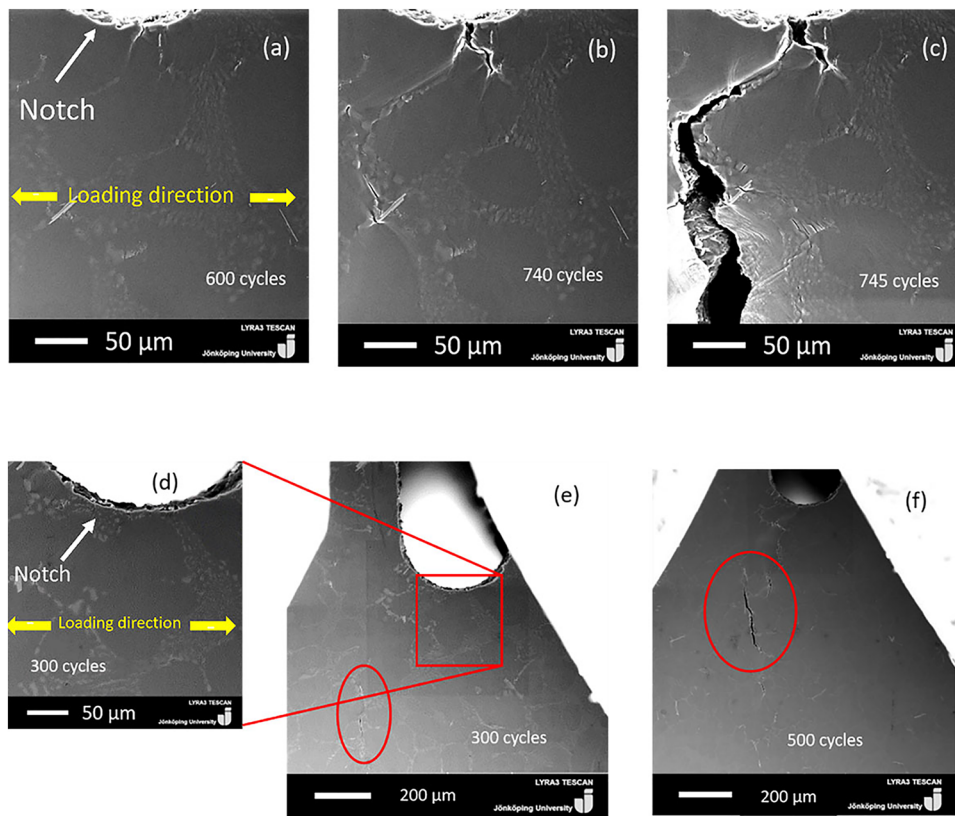
Figure 12. Crack propagation in the HIPed and heat-treated condition (a–c) the 16 mm specimen showing initiation and propagation, (d–f) the 32 mm specimen showing cracks and evaluation of crack propagation.

Conclusions

The present study aimed to describe how the defects from the casting process are affected by the HIPping process in different solidification conditions. The porosity population and coarseness before HIPping are crucial for the result of the HIPping process. The CT scanning results show that all porosities are closed. Still, the mechanical testing results, especially elongation to failure of the heat-treated material, show a significant difference between the different thicknesses.

The coarser microstructure with significantly larger porosities before the HIPping process is not healing the porosities that have been closed. The double-oxide film in the closed porosities remains like cracks hidden in the material. These bifilms assist the crack propagation, reducing static and dynamic properties. The fracture surface contains more and larger cleavage areas in the coarser fracture surface that include both Fe-rich intermetallics and bifilms.

The HIPping process, in combination with heat treatment, is beneficial in Al-Si casting up to 60 μm SDAS. In coarser microstructures, the porosities are closed and not healed, which is detrimental to the properties since they act as stress risers and assist propagation.

Open Access

REFERENCES

1. Q. Wang, D. Apelian, D. Lados, Fatigue behavior of A356-T6 aluminum cast alloys. Part I. Effect of casting defects. J. Light. Met. **1**(1), 73–84 (2001)

2. P. Osmond, L. Viet-Duc, F. Morel, D. Bellett, N. Saintier, Effect of porosity on the fatigue strength of cast aluminium alloys: from the specimen to the structure. Procedia Eng. **213**, 630–643 (2018)

3. M. Riestra, E. Ghassemali, T. Bogdanoff, S. Seifeddine, Interactive effects of grain refinement, eutectic modification and solidification rate on tensile properties of Al-10Si alloy. Mater. Sci. Eng. A **703**, 270–279 (2017)

4. S. Hegde, K.N. Prabhu, Modification of eutectic silicon in Al–Si alloys. J. Mater. Sci. **43**(9), 3009–3027 (2008)

5. B. Closset, J. Gruzleski, Mechanical properties of A356.0 alloys modified with pure strontium. AFS Trans. **90**, 453–464 (1982)

6. L. Pedersen, L. Arnberg, The effect of solution heat treatment and quenching rates on mechanical properties and microstructures in AlSiMg foundry alloys. Metall. Mater. Trans. A **32**(3), 525–532 (2001)

7. M. Brummer, H. Hoffmann, E. Werner, J. Yokohama, S. Kumai, Heat treatment of aluminum castings combined with hot isostatic pressing, in Proceedings of the 12th International Conference on Aluminium Alloys (2010)

8. M.H. Lee, J.J. Kim, K.H. Kim, N.J. Kim, S. Lee, E.W. Lee, Effects of HIPping on high-cycle fatigue properties of investment cast A356 aluminum alloys. Mater. Sci. Eng. A **340**(1–2), 123–129 (2003)

9. A. Rotella, Y. Nadot, M. Piellard, R. Augustin, M. Fleuriot, Fatigue limit of a cast Al-Si-Mg alloy (A357-T6) with natural casting shrinkages using ASTM standard X-Ray inspection. Int. J. Fatigue **114**, 177–188 (2018)

10. P. Yousefian, M. Tiryakioğlu, Pore formation during solidification of aluminum: reconciliation of experimental observations, modeling assumptions, and classical nucleation theory. Metall. Mater. Trans. A **49**, 563–575 (2018)

11. M. Tiryakioğlu, P. Yousefian, P.D. Eason, Quantification of entrainment damage in A356 aluminum alloy castings. Metall. Mater. Trans. A **49**(11), 5815–5822 (2018)

12. M. Uludağ, R. Çetin, D. Dispinar, M.J.M. Tiryakioğlu, Characterization of the effect of melt treatments on melt quality in Al-7wt% Si–Mg alloys. Metals **7**(5), 157 (2017)

13. J. Yi, Y. Gao, P. Lee, T. Lindley, Microstructure-based fatigue life prediction for cast A356-T6 aluminum-silicon alloys. Metall. Mater. Trans. B **37**(2), 301–311 (2006)

14. L. Ceschini, A. Morri, G. Sambogna, The effect of hot isostatic pressing on the fatigue behaviour of sand-cast A356-T6 and A204-T6 aluminum alloys. J. Mater. Process. Technol. **204**(1–3), 231–238 (2008)

15. H. Atkinson, S. Davies, Fundamental aspects of hot isostatic pressing: an overview. Metall. Mater. Trans. A **31**(12), 2981–3000 (2000)

16. J.T. Staley Jr., M. Tiryakioğlu, J. Campbell, The effect of hot isostatic pressing (HIP) on the fatigue life of A206-T71 aluminum castings. Mater. Sci. Eng. A **465**(1–2), 136–145 (2007)

17. S. Hafenstein, M. Brummer, M. Ahlfors, E. Werner, Combined hot isostatic pressing and heat treatment of aluminum A356 cast alloys. HTM J. Heat Treat. Mater. **71**(3), 117–124 (2016)

18. G. Ran, J. Zhou, Q. Wang, The effect of hot isostatic pressing on the microstructure and tensile properties of an unmodified A356-T6 cast aluminum alloy. J. Alloy. Compd. **421**(1–2), 80–86 (2006)

19. B. Zhou, D. Wu, Y. Ding, R. Chen, The potential application of hot isostatic pressing for magnesium alloys to reduce shrinkage porosity. Int. J. Metalcast. **17**(1), 447–454 (2023)

20. D. Apelian, S. Shivkumar, G. Sigworth, Fundamental aspects of heat treatment of cast Al–Si–Mg alloys. AFS Trans. **97**, 727–742 (1989)

21. S. Roy, L.F. Allard, A. Rodriguez, W.D. Porter, A. Shyam, Comparative evaluation of cast aluminum alloys for automotive cylinder heads: part II—mechanical and thermal properties. Metall. Mater. Trans. A **48**(5), 2543–2562 (2017)

22. E. Sjölander, S. Seifeddine, The heat treatment of Al–Si–Cu–Mg casting alloys. J. Mater. Process. Technol. **210**(10), 1249–1259 (2010)

23. T. Bogdanoff, L. Lattanzi, M. Merlin, E. Ghassemali, A.E. Jarfors, S. Seifeddine, The complex interaction between microstructural features and crack evolution during cyclic testing in heat-treated Al–Si–Mg–Cu cast alloys. Mater. Sci. Eng. **825**, 141930 (2021)

24. G.K. Sigworth, The modification of Al-Si casting alloys: important practical and theoretical aspects. Int. J. Metalcast. **2**, 19–40 (2008). https://doi.org/10.1007/BF03355425

25. L. Lu, K. Nogita, A. Dahle, Combining Sr and Na additions in hypoeutectic Al–Si foundry alloys. Mater. Sci. Eng. A **399**(1), 244–253 (2005)

26. G. Sigworth, J. Campbell, J. Jorstad, The modification of Al-Si casting alloys: important practical and theoretical aspects. Int. J. Metalcast. **3**, 65–78 (2009). https://doi.org/10.1007/BF03355442

27. C. Chama, Elimination of porosity from aluminum-silicon castings by hot isostatic pressing. J. Mater. Eng. Perform. **1**(6), 773–779 (1992)

28. S.J. Mashl, H. Bodycote, Hot Isostatic Pressing of Castings, Casting (2008)

29. Q. Wang, D. Apelian, D. Lados, Fatigue behavior of A356/357 aluminum cast alloys. Part II–Effect of

microstructural constituents. J. Light. Met. **1**(1), 85–97 (2001)

30. L. Ceschini, A. Morri, S. Toschi, S. Seifeddine, Room and high temperature fatigue behaviour of the A354 and C355 (Al–Si–Cu–Mg) alloys: role of microstructure and heat treatment. Mater. Sci. Eng. A **653**, 129–138 (2016)

31. T. Bogdanoff, J. Börjesson, S. Seifeddine, M. Tiryakioğlu, E. Ghassemali, On the secondary cracks during crack propagation in an Al–Si–Cu–Mg alloy: an in-situ study. Mater Charact **203**, 113046 (2023)